Mechanical Systems and Signal Processing, Volume 25, Issue 6, August 2011, Pages 1988-2004

Author's Accepted Manuscript

www.elsevier.com/locate/ymssp

Road vehicle state estimation using low-cost GPS/INS

King Tin Leung, James Whidborne, David Purdy, Phil Barber

PII: S0888-3270(10)00288-8
DOI: doi:10.1016/j.ymssp.2010.08.003
Reference: YMSSP 2634

To appear in: *Mechanical Systems and Signal*

Received date: 2 March 2010
Revised date: 29 June 2010
Accepted date: 11 August 2010

Cite this article as: King Tin Leung, James Whidborne, David Purdy and Phil Barber, Road vehicle state estimation using low-cost GPS/INS, *Mechanical Systems and Signal*, doi:10.1016/j.ymssp.2010.08.003

Road Vehicle State Estimation using Low-Cost GPS/INS

King Tin Leung[a], James Whidborne[a], David Purdy[b], Phil Barber[c]

[a]*School of Engineering, Cranfield University, Cranfield, UK*
[b]*Department of Engineering Systems and Management, Cranfield University, Shrivenham, UK*
[c]*Jaguar Land Rover, Whitley, Coventry, UK*

Abstract

Assuming known vehicle parameters, this paper proposes an innovative Integrated Kalman Filter (IKF) scheme to estimate vehicle dynamics, in particular the sideslip, the heading and the longitudinal velocity. The IKF is compared with the 2DoF linear bicycle model, the Triple Kalman Filter (KF) and a Model-based KF (MKF) in a simulation environment. Simulation results show that the proposed IKF is superior to other KF designs (both Kinematic KF and MKF) on state estimation when tyre characteristics are within the linear region (i.e. manoeuvres below 55kph).

Keywords: GPS, INS, Kalman filter, State estimation, Low-cost, IPG CarMaker

1. Introduction

In recent years, modern automobiles have included ever more sophisticated electronics and control systems, such as the Anti-lock Braking System (ABS) and the Electronic Stability Program (ESP). With the implementation of these intelligent systems, vehicles have become safer to drive (Van Zanten, 2002) with less involvement in fatal accidents (Farmer et al., 1997; Farmer, 2001). Evidence of this can be seen in the increased demand for ABS since 1990 (Farmer et al., 1997). It is envisaged that future development of more advanced and sophisticated control systems requires accurate and 'up-to-date' vehicle dynamic information. In particular, as highlighted by Manning and Crolla (2007), sideslip estimation is essential for a commercial viable sideslip stability control system.

Vehicle dynamic states measurement and estimation can be categorised into three main approaches. The indirect approach, which involves the use of existing in-car sensors such as the Inertial Navigation System (INS) and wheel speed sensor. This is the cheapest solution, yet suffers from accumulative integration errors due to sensor bias (Lawrence, 1998). The direct approach, includes sensors such as the speed-over-ground and Global Navigation Satellite System (GNSS), in particular the Global Positioning System (GPS). These sensors can provide accurate information but are expensive in price and to maintain. The third is the Vehicle Model (VM) approach. Although this is able to produce good estimations, VM is normally non-linear and parameter dependent. For a detailed review, see Leung et al. (2009a)

In order to obtain more accurate vehicle dynamic information, it is natural to combine the main methods in order to utilise their respective strengths. With INS and GPS in mind, Leung et al. (2009a) have identified four integrated approaches: GPS/INS, GPS/VM, INS/VM, and GPS/INS/VM. A large amount of the reported research is based on the GPS/INS Kinematic Kalman Filter (KKF) design (Bevly et al., 2000, 2001, 2002). This approach is easy to implement and is able to predict biases in the sensors. Although vehicle states can be accurately estimated with these proposed KKFs, they demand additional vehicle sensors and a high sampling-rate GPS unit. Based on a vehicle model, the GPS/VM (Bayliss et al., 2006) and the INS/VM (Best et al., 2000; Cherouat et al., 2005) are fused in a Model-based KF (MKF). Although fewer sensors are required in these designs, accurate model parameters are required. Considering the advantages of the KKF and MKF, state estimations can be further improved with an Integrated KF (IKF), which utilises GPS/INS/VM. In Anderson and Bevly (2005), Rock et al. (2005), and Best et al. (2007), the authors have used either multiple GPS antennae or expensive GPS/INS units (such as the RT3000 (OXTS, 2008)) to predict the vehicle states and model parameters. Although their designs give accurate estimations, they are generally too expensive to deploy in most production vehicles.

Although the above integrated approaches are able to estimate the vehicle dynamics, components used in the design are normally expensive specialised equipment. One of the challenges that automotive industries constantly

face is the cost-effectiveness ratio. Hence this paper proposes an IKF design that uses low-cost GPS/INS/Wheel Speed Sensors (WSS)/VM. A single antenna GPS operating at 1Hz with an accuracy of ±3m (Appendix A), is combined with existing in-car sensors (Appendix B) and WSS. The estimated states are then used in the 2 Degree of Freedom (2DoF) vehicle model to estimate the steer bias and the sideslip angles. Apart from the vehicle dynamic state estimations, this proposed IKF is also able to predict the biases in the steering wheel and the tyre radius, thereby, giving an accurate estimation of the vehicle longitudinal velocity (speed over ground).

The proposed design is tested by simulation using IPG CarMaker (aka CM) and Matlab/Simulink. Two tracks are defined in CarMaker and a virtual car based on the parameters of a Jaguar Saloon is constructed. Virtual sensors are also attached onto the virtual car and results are simulated with different driving speeds. The virtual sensor measurements are inputted in Matlab/Simulink, where noise and bias are added. Various KF designs are then tested in Matlab/Simulink to analyse their performance.

This paper is organised as follows. In the next section, a typical planar linear bicycle model is given and its relation with the GPS and INS measurements are explained. Section 3 outlines the basic formulation for a Kalman Filter (KF), the key components of the proposed IKF design are also discussed. Using the professional vehicle simulation program, IPG CarMaker, the simulation set-up is explained in Section 4. Section 5 presents the findings from the simulation. This paper finishes with conclusions and suggestions for future work.

2. Vehicle Modelling and Sensors

In a modern vehicle, the most common INS sensors used for measurements are the accelerometers and gyroscopes. To reduce cost, manufacturers often place these sensors in the longitudinal, lateral and upward direction only, thus measuring longitudinal and lateral acceleration, and yaw rate. In addition, the longitudinal velocities at the wheels can also be measured by the WSS. With the increase popularity in satellite navigation, GPS receiver has become one of the most wanted add-on device for drivers.

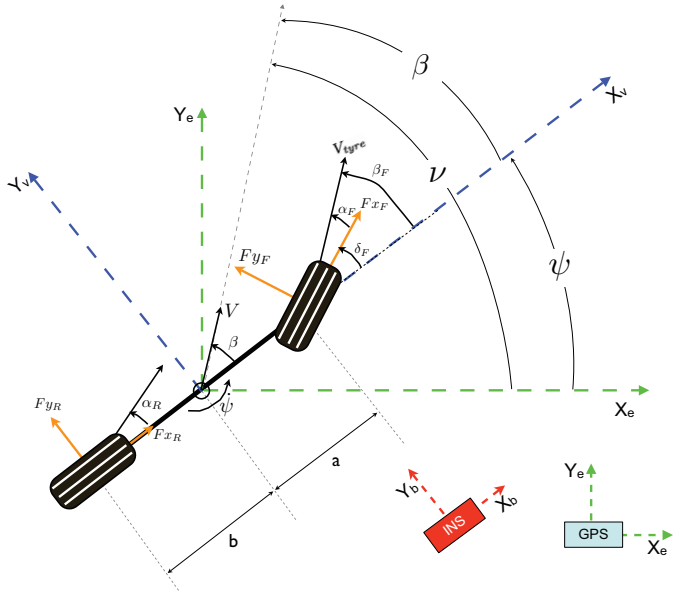

Figure 1: Typical planar bicycle model

2.1. Vehicle Sensors

Before describing the sensors that are used in this study, it is important to define each of their operating framework. Figure 1 shows a typical planar bicycle model of a four-wheeled-vehicle equipped with INS and GPS sensors. There

are normally a total of three sets of coordinate frameworks: the East North Up frame (ENU/eframe) for the GPS, the body frame (b-frame) for the INS and the ISO vehicle frame (v-frame) for the vehicle. The b-frame is rigidly attached to the vehicle body while the v-frame is fixed on the wheel/road plane. Note that although GPS often uses the North East Down (NED) frame which is standard in aerospace applications, the ENU is the ISO standard (ISO 8855) for the automotive sector.

2.1.1. Accelerometers and Gyroscopes

In Figure 1, the e-frame, b-frame and the v-frame are shown two-dimensionally with their corresponding subscripts. The majority of the INS used in ground vehicles nowadays are strap-down sensors, consisting of only two accelerometers (longitudinal and lateral) and a yaw rate gyroscope. This type of sensor moves and orientates with the vehicle, so the accelerometers and the gyro measure the accelerations (A_x, A_y) and yaw rate (r_m), respectively, in the b-frame.

The accelerometer measurements, A_x and A_y are sensitive to both translational and rotational movement of the vehicle. It is assumed here that the INS is mounted rigidly to the vehicle, and aligned perfectly along the longitudinal and lateral direction at the centre of gravity (cg). The accelerations in the b-frame on a level road without rolling or pitching motions are, hence, related to the accelerations at cg ($\ddot{x}_v$, $\ddot{y}_v$) in the v-frame by:

$$A_x = \ddot{x}_v - \dot{y}_v r_m \tag{1}$$

$$A_y = \ddot{y}_v + \dot{x}_v r_m \tag{2}$$

Note that Eqs (1) and (2) assume zero rolling and pitching in the Euler angles (i.e. ϕ, $\theta = 0$) and for the rate gyroscopes (p_m, $q_m = 0$), thus making the Euler yaw rate equal to the yaw rate gyroscopic measurements, $\dot{\psi} = r_m$, (see Leung et al. (2009a) for details). With this, the vehicle sideslip at the cg can be estimated in terms of the ratio between the lateral and longitudinal velocities,

$$\beta = \frac{\dot{y}_v}{\dot{x}_v} = \frac{\int (A_y - \dot{x}_v r_m)\mathrm{dt}}{\int (A_x + \dot{y}_v r_m)\mathrm{dt}} \tag{3}$$

Referring to Figure 1, an alternative way to obtain the sideslip and vehicle velocities in the v-frame is by transforming the accelerations measured from the sensor (b-frame) to the e-frame using the Euler angle:

$$\ddot{x}_e = A_x \cos(\psi) - A_y \sin(\psi) \tag{4}$$

$$\ddot{y}_e = A_x \sin(\psi) + A_y \cos(\psi) \tag{5}$$

To obtain the velocities and positions in the e-frame, the above equation is integrated. Using the velocities in the e-frame, the track angle (or path angle) of the vehicle, ν, can be determined as

$$\nu = \tan^{-1}\left(\frac{\dot{y}_e}{\dot{x}_e}\right) \tag{6}$$

The sideslip angle, β, is simply the difference between the track angle and the yaw angle:

$$\beta = \nu - \psi \tag{7}$$

With the sideslip calculated from Eq. (7), the vehicle velocity (v-frame) can also be derived as

$$\dot{x}_v = V \cos(\beta) \tag{8}$$

$$\dot{y}_v = V \sin(\beta) \tag{9}$$

where V is the resultant vehicle velocity with a relation of,

$$V = \sqrt{\dot{x}_e^2 + \dot{y}_e^2} = \sqrt{\dot{x}_v^2 + \dot{y}_v^2} \tag{10}$$

When a vehicle is travelling on a straight road horizontally without any side force, the sideslip angle is zero. Thus, the track angle, ν, described by the GPS coincides with the yaw angle, ψ.

2.1.2. Wheel Speed Sensors

Other than the INS and GPS, WSS can also be used for predicting the longitudinal velocity in the v-frame and the yaw rate. With a given wheel radius, R_i, and rotational speed, ω_i, the velocity of the wheel about its centre axis can be derived,

$$V_i = \omega_i R_i \tag{11}$$

where i is the position of the wheel, i.e FR, FL, RR, RL. Eq. (11) represents the longitudinal velocity under the no-slip condition. When slip occurs, the determined longitudinal velocity will be inaccurate; this error is accounted for in the KF design by the the Gaussian noise term of the WSS (see Appendix A.1).

For a vehicle, the four kinematic equations at the wheels are given as,

$$V_{FR}\cos(\delta_{FR}) = \dot{x}_v + T_F\dot{\psi} \tag{12}$$
$$V_{FL}\cos(\delta_{FL}) = \dot{x}_v - T_F\dot{\psi} \tag{13}$$
$$V_{RR} = \dot{x}_v + T_R\dot{\psi} \tag{14}$$
$$V_{RL} = \dot{x}_v - T_R\dot{\psi} \tag{15}$$

Using the above equations, the longitudinal velocity and the yaw rate at the cg can be determined. However, in order to reduce the number of dependent variables and uncertainties, only Eqs (14) and (15) are used for calculation:

$$\dot{x}_v = \frac{V_{RR} + V_{RL}}{2} = \frac{(\omega_{RR} + \omega_{RL})R_w}{2} \tag{16}$$
$$\dot{\psi} = \frac{V_{RR} - V_{RL}}{2T_R} = \frac{(\omega_{RR} - \omega_{RL})R_w}{2T_R} \tag{17}$$

From Eqs (16) and (17), while the rotational speeds are measured by the WSS, the radius, R_w, and the vehicle track distance, $2T_R$, are predetermined.

2.1.3. GPS

To date, there exists four potential GNSS providers worldwide: the American GPS, the Russian GLObal'naya NAvigatsionnaya Sputnikovaya Sistema (GLONASS), the European Galileo, and the Chinese Compass. Currently, GPS is the only fully established satellite navigation system. With a minimum of four satellites, a good position for the GPS receiver is achieved. Its velocities are then derived from the Doppler measurements (Grewal et al., 2007). As GPS is the most popular and mature GNSS provider, this paper assumes a GPS sensing system.

Using the position and velocity measurements from GPS, vehicle dynamic information can be estimated. In order to understand this, first consider the planar vehicle model in Figure 1. Assuming that a GPS receiver is located at the cg of a vehicle, its positions (x_e, y_e) and velocities $(\dot{x}_e, \dot{y}_e)$ are measured referenced to the e-frame. Using this information, the tracking angle and the resultant velocity of the vehicle can be determined by using Eqs (6) and (10) respectively.

2.2. Vehicle Modelling

Apart from using sensors to measure the vehicle dynamics, one can also use a vehicle model. Amongst the many different models, the two degrees of freedom (2DoF) model is the simplest vehicle model used for evaluating vehicle dynamics. It is based on the bicycle model as shown in Figure 1 and assumes constant longitudinal velocity, $\dot{x}_v = V$, (i.e. zero longitudinal force and zero wheel angular acceleration). Therefore, the 2DoF are the lateral motion and the rotation motion, Eqs (18) and (19) respectively. Additionally, applying the small steer angle, resulting in,

Lateral motion:

$$\ddot{y}_v = \frac{1}{m}\left(-m\dot{x}_v\dot{\psi} + F_{yF}\delta_F + F_{yR}\right) \tag{18}$$

Rotation about the vertical axis - yaw motion:

$$\ddot{\psi} = \frac{1}{J_{zz}}\left(aF_{yF} - bF_{yR}\right) \tag{19}$$

The lateral forces on the axle (i.e. F_{yF} and F_{yR}) are calculated with a tyre model. In the literature, three most common types are the linear tyre model, the Fiala tyre model (Blundell and Harty, 2004), and the 'Magic' tyre model (Bakker et al., 1989; Pacejka and Bakker, 1993; Pacejka and Besselink, 1997). For this study, the linear tyre model is used as it requires the least number of parameters with no training, thus,

$$F_{yF} = C_{yF}\alpha_F \tag{20}$$

$$F_{yR} = C_{yR}\alpha_R \tag{21}$$

The cornering coefficient for a single tyre is normally pre-determined from a tyre rig. The determined value is then doubled to give the axle cornering stiffness (i.e. C_{yF} and C_{yR}) as described in Eqs (20) and (21). This is because the test on the tyre rig only accounts for a single tyre.

The slip angles (i.e. α_F and α_R) as shown in Figure 1 are defined as the difference between the sideslip angle and the steering angle at the tyres. Note that the sideslip at the tyres is not the same as that at the cg, β, due to the difference in velocities at the tyres. Therefore, applying the small sideslip assumption, slip at the tyres can be approximated as,

$$\begin{aligned} \alpha_F &= \beta_F - \delta_F \\ &\approx \frac{\dot{y}_v + a\dot{\psi}}{\dot{x}_v} - \delta_F = \beta + \frac{a\dot{\psi}}{\dot{x}_v} - \delta_F \end{aligned} \tag{22}$$

$$\begin{aligned} \alpha_R &= \beta_R \\ &\approx \frac{\dot{y}_v - b\dot{\psi}}{\dot{x}_v} = \beta - \frac{b\dot{\psi}}{\dot{x}_v} \end{aligned} \tag{23}$$

Combining Eqs (20) to (23), substituting them into the two equations of motion, Eqs (18) and (19), and finally approximating $\ddot{y}_v \approx \dot{\beta}\dot{x}_v$, the state space representation for the 2DoF linear bicycle model becomes:

$$\begin{bmatrix} \dot{\beta} \\ \ddot{\psi} \end{bmatrix} = \begin{bmatrix} \frac{C_{yF}+C_{yR}}{mV} & \frac{aC_{yF}-bC_{yR}}{mV^2} - 1 \\ \frac{aC_{yF}-bC_{yR}}{J_{zz}} & \frac{a^2C_{yF}-b^2C_{yR}}{J_{zz}V} \end{bmatrix} \begin{bmatrix} \beta \\ \dot{\psi} \end{bmatrix} + \begin{bmatrix} \frac{-C_{yF}}{mV} \\ \frac{-aC_{yF}}{J_{zz}} \end{bmatrix} \delta_F \tag{24}$$

From the state-space model in Eq. (24), the input is the tyre steering angle, δ_F and the states are the sideslip and the yaw rate, $\begin{bmatrix} \beta & \dot{\psi} \end{bmatrix}^T$. This model is very popular with automotive manufacturers as it is simple, easy to implement and requires relatively few parameters. In practice, the velocity, V, in the equation is normally measured from the WSS.

3. The Kalman Filter Design

Prior to presenting the proposed design of the IKF, the KF and Extended KF (EKF) are summarised. Details can be found in, for example, Welch and Bishop (2001). The Triple KF, comprising of three KKFs (two linear and one non-linear), is then described. The section finishes with an overview of the MKF and a description of the IKF.

3.0.1. The Kalman Filter

Given the discrete plant model, $\mathrm{x_{k+1}} = \mathbf{\Phi_k}\mathrm{x_k} + \mathbf{\Delta_k}\mathrm{u_k}$, with measurements, $\mathrm{z_k} = \mathbf{H_k}\mathrm{x_k}$, and assuming Gaussian process and measurement noise, $\mathbf{\Gamma}_k\mathrm{w_k}$ and $\mathrm{v_k}$ respectively, a Linear KF (LKF) can be applied. In general, the KF is a

two-stage process consisting of the correction and the prediction stages:
Correction stage:

$$\hat{z}_k = \mathbf{H}_k \hat{x}_{k|k-1} \tag{25}$$

$$\mathbf{K}_k = \mathbf{P}_{k|k-1}\mathbf{H}_k(\mathbf{H}_k\mathbf{P}_{k|k-1}\mathbf{H}_k^T + \mathbf{R}_k)^{-1} \tag{26}$$

$$\mathbf{P}_{k|k} = (\mathbf{I} - \mathbf{K}_k\mathbf{H}_k)\mathbf{P}_{k|k-1} \tag{27}$$

$$\hat{x}_{k|k} = \hat{x}_{k|k-1} + \mathbf{K}_k(z_k - \hat{z}_k) \tag{28}$$

Prediction stage:

$$\hat{x}_{k+1|k} = \mathbf{\Phi}_k \hat{x}_{k|k} + \mathbf{\Delta}_k u_k \tag{29}$$

$$\mathbf{P}_{k+1|k} = \mathbf{\Phi}_k\mathbf{P}_{k|k}\mathbf{\Phi}_k^T + \mathbf{\Gamma}_k\mathbf{Q}_k\mathbf{\Gamma}_k^T \tag{30}$$

At time step k, the inputs to a LKF are the state variables estimated from the previous time step, $\hat{x}_{k|k-1}$, and, the primary and referenced sensor measurements, u_k and z_k. Firstly, the referenced measurements, $\hat{z}_k$, are predicted using the current estimated state variables, Eq. (25). These predicted reference measurements are then compared with the actual measured reference value, $z_k - \hat{z}_k$. Their error is then multiplied by a weighing matrix called the Kalman gain, $\mathbf{K}_k$, and the old estimated states are updated using Eq. (28). Using the updated state estimations, $\hat{x}_{k|k}$, and the system equations, the states for the next time step, $k + 1$, are predicted using Eq. (29). At time step $k + 1$, the estimated states from Eq. (29) are inserted into Eq. (25) and the process repeats.

Although the LKF is simple to implement, in reality, most systems are non-linear and in such cases, an EKF can be applied. Consider the non-linear discretized system :

$$\begin{aligned}\hat{x}_{k+1} &= \hat{x}_k + T_s\mathbf{f}(\hat{x}_k, u_k, w_k) \\ &= \hat{\mathbf{f}}(\hat{x}_k, u_k, w_k)\end{aligned} \tag{31}$$

$$\hat{z}_k = \mathbf{g}(\hat{x}_k, v_k) \tag{32}$$

The EKF is implemented similarly to the LKF, with the following two stages:
Correction stage:

$$\hat{z}_k = \mathbf{g}(\hat{x}_{k|k-1}, 0) \tag{33}$$

$$\mathbf{K}_k = \mathbf{P}_{k|k-1}\mathbf{G}_k(\mathbf{G}_k\mathbf{P}_{k|k-1}\mathbf{G}_k^T + \mathbf{R}_k)^{-1} \tag{34}$$

$$\mathbf{P}_{k|k} = (\mathbf{I} - \mathbf{K}_k\mathbf{G}_k)\mathbf{P}_{k|k-1} \tag{35}$$

$$\hat{x}_{k|k} = \hat{x}_{k|k-1} + \mathbf{K}_k(z_k - \hat{z}_k) \tag{36}$$

Prediction stage:

$$\hat{x}_{k+1|k} = \hat{\mathbf{f}}(\hat{x}_{k|k}, u_k, 0) \tag{37}$$

$$\mathbf{P}_{k+1|k} = \mathbf{F}_k\mathbf{P}_{k|k}\mathbf{F}_k^T + \mathbf{\Gamma}_k\mathbf{Q}_k\mathbf{\Gamma}_k^T \tag{38}$$

where matrices, $\mathbf{F}$ and $\mathbf{G}$, are the partial derivatives (Jacobian matrices) of the process and measurement functions, $\hat{\mathbf{f}}$ and $\mathbf{g}$ respectively:

$$\mathbf{F}_{[i][j]} = \frac{\delta\hat{\mathbf{f}}_{[i]}}{\delta x_{[j]}}(\hat{x}_k, u_k, 0) \tag{39}$$

$$\mathbf{G}_{[i][j]} = \frac{\delta\mathbf{g}_{[i]}}{\delta x_{[j]}}(\hat{x}_k, 0) \tag{40}$$

3.1. The Triple Kalman Filter

From the literature, the most simple and straight forward GPS/INS KF design is the dual KF (comprising two KKF which estimates the heading angle and the vehicle velocities) set up given by Bevly et al. (2000, 2001), and Ryu et al. (2002). With an additional KF utilising the WSS, the dual KF is modified to form the Triple KF design.

3.1.1. The Yaw Kalman Filter, yawKKF

The dual KF approach is suitable for car manufacturers as it is not dependent on vehicle parameters, such as mass, inertia and tyre coefficients. The *yawKKF* consists of a state vector of two states: heading angle, ψ, and yaw rate gyro bias, b_r. The measurement for the *yawKKF* is taken from the GPS tracking angle only, ν, and is related to the heading only when the vehicle is travelling on a straight road: $\nu = \psi$. This is because vehicles generate a sideslip angle only during cornering, making the tracking angle equal to the sum of the heading and sideslip angles: $\nu = \psi + \beta$. Therefore, the measurement for this KKF switches on and off depending on two circumstances:

1. the presence of GPS signals, and
2. whether the vehicle is traveling straight or not.

The presence of GPS signals is often detected by a GPS tag sent from the receiver and the determination of vehicle cornering can be determined from the yaw rate gyro or the steering wheel sensor. We propose using the former as rate gyro bias can be estimated using a simple *yawKKF*.

After the states are estimated from the *yawKKF*, the yaw rate measurements are corrected ($r_m - \hat{b}_r$) and the estimated heading angle is combined with the GPS tracking angle and velocity to produce the longitudinal and lateral velocities in the v-frame as reference measurements for the *velKKF*:

$$\dot{x}_v^{ref} = V_{gps}\cos(\nu_{gps} - \hat{\psi}) \tag{41}$$

$$\dot{y}_v^{ref} = V_{gps}\sin(\nu_{gps} - \hat{\psi}). \tag{42}$$

Using these reference measurements, the *velKKF* predicts the longitudinal and lateral velocities in b-frame as well as the biases in the corresponding accelerometers. A summary for the *yawKKF* is presented below:

$$\begin{bmatrix}\psi \\ b_r\end{bmatrix}_{k+1} = \begin{bmatrix}1 & -T_s \\ 0 & 1\end{bmatrix}\begin{bmatrix}\hat{\psi} \\ \hat{b}_r\end{bmatrix}_k + \begin{bmatrix}T_s \\ 0\end{bmatrix}\begin{bmatrix}r_m\end{bmatrix}_k \tag{43}$$

$$\begin{bmatrix}\nu\end{bmatrix}_k = \mathbf{H_{yaw}}\begin{bmatrix}\hat{\psi} \\ \hat{b}_r\end{bmatrix}_k \tag{44}$$

where $\mathbf{H_{yaw}}$ is $\begin{bmatrix}1 & 0\end{bmatrix}$ when the GPS is available travelling on a straight road, or $\begin{bmatrix}0 & 0\end{bmatrix}$ when either GPS is off or the vehicle is turning.

In order to 'correctly' determine the sideslip angle, the GPS tracking angle must be properly synchronised with the heading estimate from the *yawKKF* in the same numerical range. To do this, the two angles are converted to the trigonometric numerical range before making comparison. Hence the measurement expression in Eq. (44) is no longer a direct comparison with the GPS tracking angle, i.e. $\nu_k = \hat{\psi}_k$, but a non-linear trigonometric relationship,

$$\begin{bmatrix}\cos\nu \\ \sin\nu\end{bmatrix}_k = \begin{bmatrix}\cos\hat{\psi} \\ \sin\hat{\psi}\end{bmatrix}_k.$$

This change causes the simple measurement matrix, $\mathbf{H_{yaw}}$, to be replaced by a non-linear Jacobian matrix, $\mathbf{G_{yaw}}$, in the KF formulation:

$$\mathbf{G_{yaw}}^{i,j} = \left[\frac{\partial z_i}{\partial x_j}\right]^{i,j=1,2} = \begin{bmatrix}-\sin\hat{\psi}_k & 0 \\ \cos\hat{\psi}_k & 0\end{bmatrix}. \tag{45}$$

In the absence of GPS signals, the measurement matrix, $\mathbf{G_{yaw}}$, becomes zero.

3.1.2. The WSS Kalman Filter, wssEKF

In Section 2.1, it shows that WSS measurements can be used for estimating the longitudinal velocity, $\dot{x}_v$, and the yaw rate, $\dot{\psi}$ (see Eqs (16) and (17)). However, due to errors in the wheel rotational speed and tyre radius, the WSS measurements are not accurate enough to be used, hence a KF is utilised, i.e. *wssEKF*.

The purpose of the *wssEKF* in the Triple KF design is to predict the tyre radius bias and therefore the longitudinal velocity. This is because the predicted longitudinal velocity is more accurate with less noise from *wssEKF* when compared with the dual KF design in Leung et al. (2008), see Figure 2. To construct the *wssEKF*, the WSS formulations

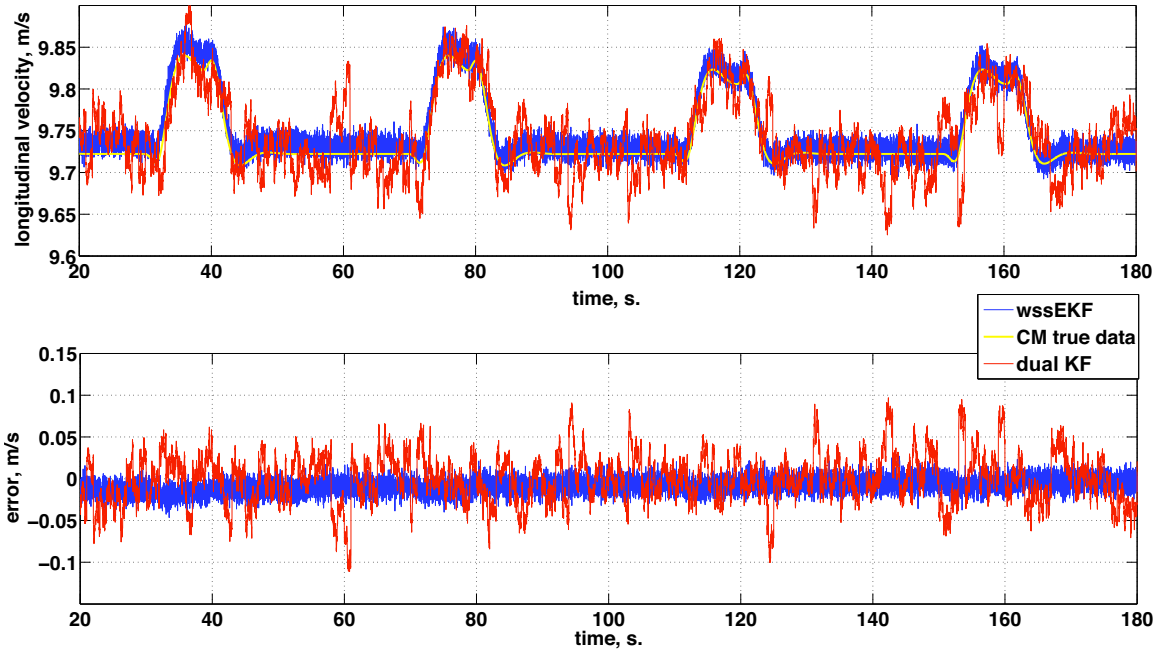

Figure 2: Comparison of longitudinal state estimation from *wssEKF* and dual KF, with actual longitudinal velocity from CarMaker (labelled CM true data) in *DoubleOval_25kph*

in Eqs (16) and (17) are first discretised to,

$$x_v^{k+1} = x_v^k + T_s\left(\frac{1}{2}(\omega_{RR} + \omega_{RL})(R_w + b_w)\right) \tag{46}$$

$$\psi^{k+1} = \psi^k + T_s\left(\frac{1}{2T_R}(\omega_{RR} - \omega_{RL})(R_w + b_w)\right) \tag{47}$$

Using Eq. (47) only, the *wssEKF* is constructed with a process matrix of,

$$\begin{bmatrix}\psi \\ b_w\end{bmatrix}_{k+1} = \begin{bmatrix}1 & \frac{T_s}{2T_R}(\omega_{RR} - \omega_{RL}) \\ 0 & 1\end{bmatrix}\begin{bmatrix}\psi \\ b_w\end{bmatrix}_k + \begin{bmatrix}\frac{T_s}{2T_R}(\omega_{RR} - \omega_{RL}) \\ 0\end{bmatrix}R_w.$$

With the measurements from the GPS (v) and *yawKKF* ($\hat{\psi}_{yawKKF}$), the measurement matrix of *wssEKF* is varied according to three conditions,

$$\begin{bmatrix}\cos(v_{gps}) \\ \sin(v_{gps}) \\ b_{w|gps} \\ \cos(\hat{\psi}_{yawKKF}) \\ \sin(\hat{\psi}_{yawKKF})\end{bmatrix}_k = \mathbf{g_{wss}}\,(\psi, b_w)_k \tag{48}$$

1. Corners (when corrected $\dot{\psi} > 2°$ /s):

$$\mathbf{G_{wss}} = \frac{\partial \mathbf{g_{wss}}}{\partial \mathbf{x}_k} = \begin{bmatrix}0 & 0 & 0 & 0 & 0 \\ 0 & 0 & 0 & -\sin(\psi) & \cos(\psi)\end{bmatrix}_k^T \tag{49}$$

2. Straight road and GPS is 'ON':

$$\mathbf{G_{wss}} = \frac{\partial \mathbf{g_{wss}}}{\partial \mathbf{x}_k} = \begin{bmatrix} 0 & 0 & 1 & 0 & 0 \\ -\sin(\psi) & \cos(\psi) & 0 & 0 & 0 \end{bmatrix}_k^T \tag{50}$$

3. Straight road and GPS is 'OFF':

$$\mathbf{G_{wss}} = \frac{\partial \mathbf{g_{wss}}}{\partial \mathbf{x}_k} = \begin{bmatrix} 0 & 0 & 1 & 0 & 0 \\ 0 & 0 & 0 & 0 & 0 \end{bmatrix}_k^T \tag{51}$$

Notice that the wheel bias is also measured by the GPS, by assuming the wheel velocity is the same as the GPS speed on a straight road, therefore,

$$\begin{aligned} \dot{x}_v|_{straight} \approx V_{gps} &= \frac{(\omega_{RR} + \omega_{RL})(R_w + b_w)}{2} \\ b_w &= \frac{2V_{gps}}{\omega_{RR} + \omega_{RL}} - R_w = b_{w|gps}. \end{aligned} \tag{52}$$

Once the bias of the WSS is determined, the longitudinal velocity is determined by,

$$x_v^{wssEKF} = \left(\frac{1}{2}(\omega_{RR} + \omega_{RL})(R_w + b_w) \right) \tag{53}$$

3.1.3. The Velocity Kalman Filter, velKKF

With the yaw rate bias and longitudinal velocity estimated from the *yawKKF* and the *wssEKF* respectively, they are used in the *velKKF* along with the GPS measurements to produce an improved estimation for the velocities, the accelerometer biases, b_x and b_y, and also the error caused by the pitching motion, b_d. As a result, Eqs (1) and (2) are modified to:

$$A_x = \ddot{x}_v - \dot{y}_v r_m + b_x + b_d \tag{54}$$

$$A_y = \ddot{y}_v + \dot{x}_v r_m + b_y \tag{55}$$

which correspond to a state space representation of:

$$\begin{bmatrix} \dot{x}_v \\ b_x \\ \dot{y}_v \\ b_y \\ b_d \end{bmatrix} = \begin{bmatrix} 0 & -1 & (r_m - \hat{b_r}) & 0 & -1 \\ 0 & 0 & 0 & 0 & 0 \\ -(r_m - \hat{b_r}) & 0 & 0 & -1 & 0 \\ 0 & 0 & 0 & 0 & 0 \\ 0 & 0 & 0 & 0 & 0 \end{bmatrix} \begin{bmatrix} \dot{x}_v \\ b_x \\ \dot{y}_v \\ b_y \\ b_d \end{bmatrix} + \begin{bmatrix} 1 & 0 \\ 0 & 0 \\ 0 & 1 \\ 0 & 0 \\ 0 & 0 \end{bmatrix} \begin{bmatrix} A_x \\ A_y \end{bmatrix}_k \tag{56}$$

$$\begin{bmatrix} \dot{x}_v^{ref} \\ \dot{y}_v^{ref} \\ z_3^{ref} \end{bmatrix} = \begin{bmatrix} 1 & 0 & 0 & 0 & 0 \\ 0 & 0 & 1 & 0 & 0 \\ & (\mathbf{h_{vel,3}})_{1\times 5} & & & \end{bmatrix} \begin{bmatrix} \dot{x}_v \\ b_x \\ \dot{y}_v \\ b_y \\ b_d \end{bmatrix}_k \tag{57}$$

where $\dot{x}_v^{ref}$ and $\dot{y}_v^{ref}$ are determined from Eqs (41) and (42) using the estimated heading angle from the *yawKKF* and the GPS tracking angle.

When GPS is unavailable, it is recommended in Leung et al. (2009b) that the measurement matrix must remain 'ON' instead of turning the matrix into zeros. The measurement covariance for the *velKKF*, $\mathbf{R_{vel}}$, is thus set to a large value (as listed in Appendix A.2), reducing the effect of the measurements on the estimated states. In addition, during GPS outages, longitudinal velocity estimation from *wssEKF* is used as a continual source of measurement for the *velKKF*.

The pitching acceleration error, b_d, can be estimated by assuming it to be zero on the straight road and equal to the difference between the GPS velocity (Eq. (41)) and the WSS velocity (Eq. (53)) over one GPS sample period (T_s^{gps}) on the curve:

1. Straight:

$$\begin{cases} b_d = 0 \\ z_3^{ref} = \dot{x}_v^{wssEKF} \\ \mathbf{h}_{\mathbf{vel},3} = \begin{bmatrix} 1 & 0 & 0 & 0 & 0 \end{bmatrix} \end{cases} \tag{58}$$

2. Curve and when GPS is available:

$$\begin{cases} b_d = \dfrac{1}{T_s^{gps}} \left(\dot{x}_v^{ref} - \dot{x}_v^{wssEKF} \right) \\ z_3^{ref} = \dot{x}_v^{ref} - \dot{x}_v^{wssEKF} \\ \mathbf{h}_{\mathbf{vel},3} = \begin{bmatrix} 0 & 0 & 0 & 0 & T_s^{gps} \end{bmatrix} \end{cases} \tag{59}$$

3. Curve and when GPS is not available:

$$\begin{cases} b_d = \dfrac{1}{T_s^{gps}} \left[\dot{x}_v - \dot{x}_v^{wssEKF} \right] \\ z_3^{ref} = \dot{x}_v^{wssEKF} \\ \mathbf{h}_{\mathbf{vel},3} = \begin{bmatrix} 1 & 0 & 0 & 0 & -T_s^{gps} \end{bmatrix} \end{cases} \tag{60}$$

3.2. *The Integrated Kalman Filter, IKF*

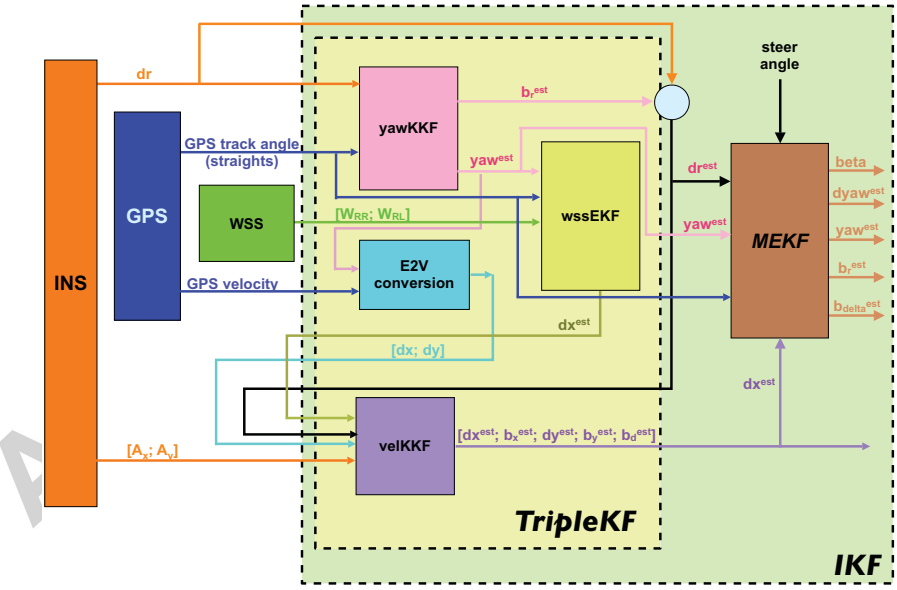

Figure 3: Schematic diagram for the Triple KF and the IKF design

The IKF design combines an MEKF with the Triple KF described in Section 3.1, see Figure 3. In the Triple KF, while the *yawKKF* provides a good continual heading angle estimation, the *wssEKF* gives a good estimation for the longitudinal velocity. Together, the two KFs allow a continuous estimation of vehicle velocities in the *velKKF* regardless of the GPS outages. This longitudinal velocity estimation from the *velKKF* and the corrected yaw rate from the *yawKKF* are then fed into the *MEKF* to estimate the vehicle dynamic states.

3.2.1. The Model-based Kalman Filter

The MEKF design is based on the 2DoF linear bicycle model, Eq. (24). As state estimations using the vehicle model are sensitive to the steering input, it is essential to ensure that the steering input is correct with the bias, b_δ, compensated. To achieve this, b_δ is added onto the state vector. Furthermore, the MEKF is also accommodated with the ability to estimate the bias from the yaw rate gyroscope. The state space representation for the MEKF is thus,

$$\begin{bmatrix} \dot{\beta} \\ \ddot{\psi} \\ \dot{\psi} \\ \dot{b}_r \\ \dot{b}_\delta \end{bmatrix} = \begin{bmatrix} \frac{C_{yF}+C_{yR}}{mV} & \frac{aC_{yF}-bC_{yR}}{mV^2}-1 & 0 & 0 & \frac{-C_{yF}}{mV} \\ \frac{aC_{yF}-bC_{yR}}{J_z} & \frac{a^2C_{yF}+b^2C_{yR}}{J_zV} & 0 & 0 & \frac{-aC_{yF}}{J_z} \\ 0 & 1 & 0 & 0 & 0 \\ 0 & 0 & 0 & 0 & 0 \\ 0 & 0 & 0 & 0 & 0 \end{bmatrix} \begin{bmatrix} \hat{\beta} \\ \hat{\dot{\psi}} \\ \hat{\psi} \\ \hat{b}_r \\ \hat{b}_\delta \end{bmatrix} + \begin{bmatrix} \frac{-C_{yF}}{mV} \\ \frac{-aC_{yF}}{J_z} \\ 0 \\ 0 \\ 0 \end{bmatrix} \delta_F. \tag{61}$$

In dependent on the availability of GPS signal, the MEKF is updated with the measurements from the yaw rate gyroscope, r_m, and the GPS tracking angle, ν, such that,

$$\begin{cases} r_m = \hat{\dot{\psi}} + \hat{b}_r \\ \cos\nu = \cos(\hat{\psi} + \hat{\beta}) \\ \sin\nu = \sin(\hat{\psi} + \hat{\beta}) \end{cases} \tag{62}$$

In addition, due to the inaccuracy of estimating the steer bias in the MEKF during vehicle cornering ($r_m > 2^\circ/s$), a 10 seconds equal weighted moving average window is applied on the steer bias to supply the MEKF with a smooth bias prediction.

4. The Simulation

Proposed design is tested by simulations carried out in MATLAB/Simulink. GPS, INS and vehicle models are built in Simulink and the KF designs are written in MATLAB code. The inputs of the simulations are gathered from a commercial simulation programme called IPG CarMaker. Noise and disturbances are added onto the inputs before processing through the sensor models and KF designs. The estimated results are then compared with the measurements from CarMaker, and errors are calculated as Eqs (63) and (64).

4.1. Vehicle and Sensor parameters

The vehicle parameters are based on a Jaguar Saloon. Data for this vehicle can be found in Appendix B. Because this study is concerned about the performance of using low-cost sensors, the INS and GPS is thus operated at a sampling frequency of 100Hz and 1Hz respectively.

In the simulation, it is assumed that sensors are located at the cg of the vehicle. Sensor noise is assumed as white with a constant bias (as specified in Appendix A). These errors are added to the corresponding INS measurements and passed through a CAN-bus simulator, before being used in the KF designs. As the GPS is an add-on device, its measurements are fed into the KFs directly without going through the CAN-bus.

4.2. The Tracks

In this study, two different tracks are used for simulations. They are described as follows,

1. the *DoubleOval* – two oval shaped tracks, one turning left and the other one turning right;
2. the *LaneChangeISO* – a double lane change, which turns right and then left again.

4.3. Error calculations

To compare the estimations of the different KF designs and their effectiveness on various roads and manoeuvres, the error of the estimated states are determined with the reference measurement from CarMaker. This error is derived using the Root Mean Squared Deviation (RMSD) or the Normalised RMSD (NRMSD), which describes the amount of deviation of the estimated states (X_i^{est}) from the true value (X_i^t), given by the following relationship:

$$\%RMSD = \sqrt{\frac{\sum_{i=1}^{N}(X_i^{est} - X_i^t)^2}{N}} \times 100\% \tag{63}$$

$$\%NRMSD = \frac{\%RMSD}{(X_{max}^t - X_{min}^t)} \tag{64}$$

where N is the total number of data points, X_{max}^t is the maximum of the true data set, and X_{min}^t is the minimum of the true data set.

The NRMSD is a useful error measuring tool for any time-varying dynamic state, i.e. the yaw rate, the lateral velocity and the sideslip, while the RMSD is suitable for any states which are assumed as near constant, such as the vehicle speed and the bias of the sensors.

5. Results and Discussion

With the 2 simulated tracks (*DoubleOval* and *LaneChangeISO*), 10 manoeuvres are carried out with speed varying from 15kph to 55kph. These speeds are chosen so the tyre dynamics remain in the linear region. For each manoeuvre, 10 simulations are performed and an average error is determined. The bias estimation ability of the IKF is first discussed, and then the performance of vehicle dynamic state estimations.

5.1. Bias Estimation

Table 1: Bias estimation errors (%RMSD) for the IKF and DKF

		yawKKF		***velKKF***				***wssEKF***	**MEKF**
		IKF	DKF	IKF	DKF	IKF	DKF	IKF	IKF
	Estimated bias states:	$\hat{b}_r$	$\hat{b}_r$	$\hat{b}_x$	$\hat{b}_x$	$\hat{b}_y$	$\hat{b}_y$	$\hat{b}_w$	$\hat{b}_\delta$
manoeuvre	*DoubleOval_15kph*	0.04	0.08	13.14	13.96	0.21	0.22	0.34	0.08
	DoubleOval_25kph	0.06	0.08	13.15	15.18	0.38	0.16	0.37	0.06
	DoubleOval_35kph	0.09	0.08	13.21	17.35	0.40	0.41	0.31	0.05
	DoubleOval_45kph	0.05	0.09	13.85	20.03	0.79	0.57	0.08	0.05
	DoubleOval_55kph	0.08	0.09	13.68	23.22	1.29	1.08	0.24	0.07
	LaneChangeISO_15kph	0.09	0.09	2.31	0.49	0.14	0.44	0.25	0.13
	LaneChangeISO_25kph	0.08	0.10	2.69	3.24	0.58	0.46	0.31	0.08
	LaneChangeISO_35kph	0.16	0.23	12.81	23.55	0.91	1.07	0.20	0.08
	LaneChangeISO_45kph	0.18	0.16	12.65	30.46	1.27	1.48	0.32	0.07
	LaneChangeISO_55kph	0.25	0.21	12.74	39.09	2.19	2.06	0.38	0.07

Table 1 shows the bias estimation errors for the IKF and the DKF designs. Inspecting the bias estimations of the IKF, it is clear that all bias are well estimated with a %RMSD below 1%, except the longitudinal accelerometer bias, b_x. The inability of predicting b_x accurately is due to the constant velocity (i.e. negligible acceleration) manoeuvre in the simulations.

For the DKF design, the bias estimations are very similar to those from the IKF with no significant difference apart from the longitudinal accelerometer bias. This difference is due to the longitudinal measurements in the KF designs. Recall that longitudinal estimation in the DKF uses measurements from the GPS, while that in the IKF uses longitudinal estimations from the *wssEKF*. The precise wheel bias, b_w, estimation from the *wssEKF* allows the longitudinal velocity to be predicted more accurately in the IKF overall.

Table 2: State estimation error of Triple KF, IKF and Solo MEKF, %NRMSD

	sideslip, $\hat{\beta}$			**yaw rate, $\hat{\psi}$**		
Manoeuvre	Triple KF	IKF	Solo MEKF	Triple KF	IKF	Solo MEKF
DoubleOval_15kph	6.8045	0.4174	0.6062	0.7560	0.4377	0.8362
DoubleOval_25kph	5.2610	0.3232	0.8253	0.4946	0.3555	0.5631
DoubleOval_35kph	6.9596	0.5600	1.2146	0.3849	0.3683	0.3609
DoubleOval_45kph	15.1912	4.0282	3.5376	0.3259	0.3511	0.2580
DoubleOval_55kph	12.7709	12.8077	10.1776	0.2911	0.7194	0.7895
LaneChangeISO_15kph	21.0481	1.8495	2.3481	2.6157	1.8660	2.1964
LaneChangeISO_25kph	17.8751	1.4995	2.3685	2.109	1.4815	2.0595
LaneChangeISO_35kph	17.2353	1.4223	1.9844	1.7858	1.2260	1.6298
LaneChangeISO_45kph	24.3931	2.2926	2.7409	1.5617	1.0856	1.4280
LaneChangeISO_55kph	69.7912	9.2321	9.8130	1.4422	0.99748	1.2488

5.2. Sideslip and Yaw Rate estimation

Figure 4 shows the longitudinal velocity inputs of the MEKF working alone (Solo MEKF) and the MEKF of the IKF. The Solo MEKF uses the longitudinal velocity determined from the WSS as inputs, while the IKF MEKF uses longitudinal velocity estimations from the *velKKF*. Comparing the two velocities, it is clear that the IKF MEKF has a better longitudinal velocity input. The benefit of the accurate longitudinal velocity determination is shown in Table 2, in which both sideslip and yaw rate estimations are more accurate when the linear cornering coefficients are applicable to the 2DoF bicycle model (i.e. *DoubleOval_15kph* to *DoubleOval_35kph* and *LaneChangeISO_15kph* to *LaneChangeISO_55kph*). For manoeuvres which do not have a linear lateral tyre force to slip behaviour, Table

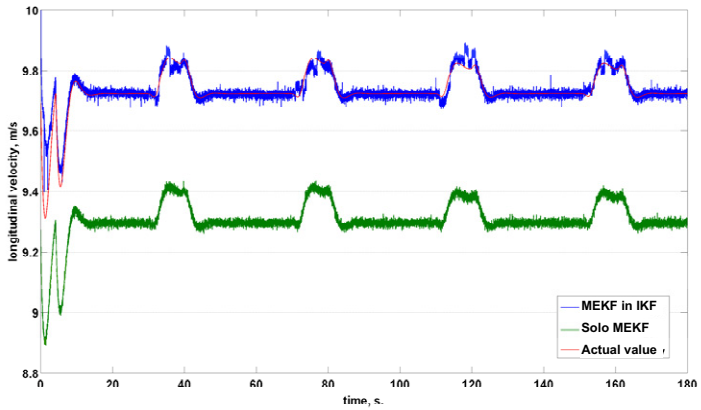

Figure 4: Longitudinal velocity inputs to the Solo MEKF and the MEKF in IKF in the *DoubleOval_35kph* manoeuvre

2 shows that the state estimations are more accurate with the Solo MEKF. This result is due to the compensation between parametric errors and state estimation errors.

Referring to the yaw rate estimation in the Triple KF and the Solo MEKF, Table 2, we can see that the Triple KF is able to provide an accurate heading and longitudinal velocity while the Solo MEKF is good at estimating fast dynamic change of the vehicle (i.e. relatively low %NRMSD for the *LaneChangeISO* manoeuvres). By utilising these advantages from the two approaches, the IKF gives the most accurate state estimations when the linear 2DoF bicycle model is valid.

Figures 5 to 6 shows the errors of the sideslip and heading estimations of different estimation approaches, namely the IKF, the Solo MEKF, the Triple KF and the original linear 2DoF bicycle model. Results for the two manoeuvres with valid linear 2DoF vehicle model, i.e. *DoubleOval_35kph* and *LaneChangeISO_35kph* are presented here.

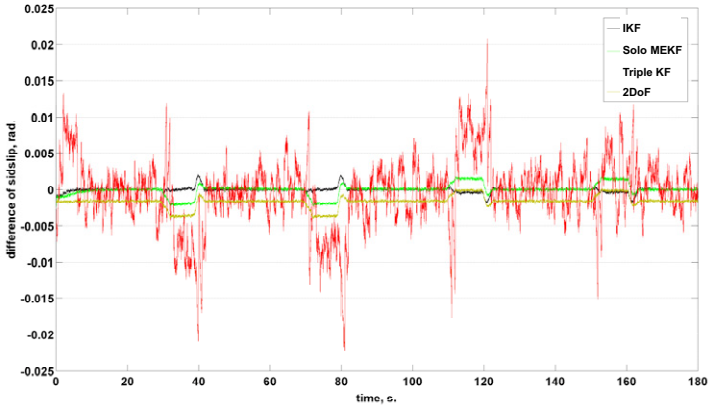

(a) Error in sideslip angle estimations

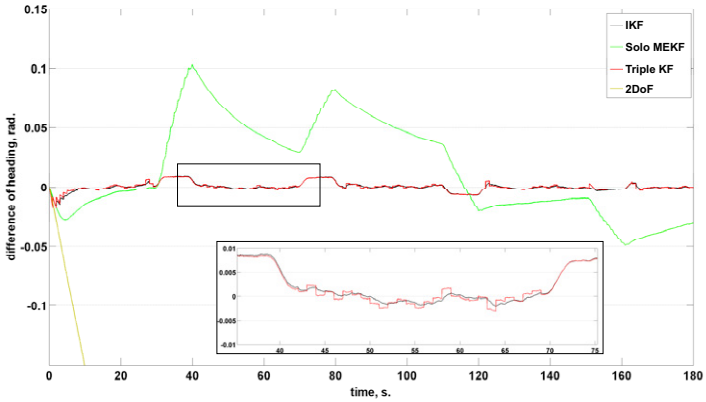

(b) Error in heading angle estimations

Figure 5: State estimation errors of *DoubleOval_35kph* manoeuvre with different estimation approaches

Figure 5 shows the state estimation errors from when the vehicle is travelling on the *DoubleOval_35kph* manoeuvre. For the sideslip estimation, Figure 5a reveals that the Triple KF provides a noisy estimation, which is due to the inaccuracy of lateral velocity estimation in the *velKKF*. On the other hand, approaches based on the vehicle model are able to give more stable estimations. However, without any error feedback and bias estimation algorithm, the 2DoF vehicle model estimates the sideslip with an offset. When KF is introduced into the 2DoF model, i.e. the Solo MEKF, the offset is compensated but during corners, sideslip errors increase. Notice that the sideslip estimation of the Solo MEKF and the 2DoF model are almost the same but with an offset. For the third and fourth corners, where the vehicle is turning right, the offset error of the 2DoF model has become beneficial to the sideslip estimation. This 2DoF result is only good for this particular simulation and cannot be used as a general explanation for all vehicle systems. The most accurate sideslip estimation is produced by combining the Triple KF with the Solo MEKF, i.e. IKF. Whether the vehicle is travelling straight or cornering, the sideslip is predicted accurately with small overshoots just before the vehicle exits the corner.

For the heading estimations, Figure 5b shows that the 2DoF vehicle model has increasing errors due to the biases from the yaw rate gyroscope and steering wheel. Even with the bias predicted, Figure 5b shows that the Solo MEKF is not able to track the heading of the vehicle accurately, but bounds the errors. As the Triple KF manages to predict the yaw rate and heading accurately, when utilising these estimations in the IKF, the heading estimations are as accurate as those predicted from the Triple KF. In fact, from the zoom-in region of the graph, it can be seen that the IKF provides

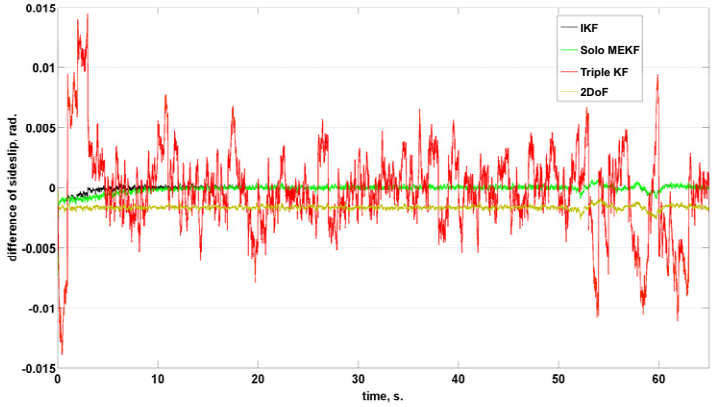

(a) Error in sideslip angle estimations

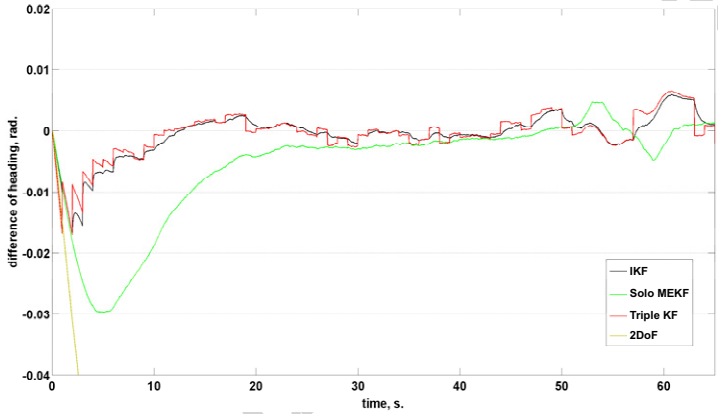

(b) Error in heading angle estimations

Figure 6: State estimation errors of *LaneChangeISO_35kph* manoeuvre with different estimation approaches

smoother heading estimations than the Triple KF.

For fast dynamic manoeuvres such as the *LaneChangeISO_35kph*, Figure 6a shows that the sideslip estimation is not accurately predicted when solely using the Triple KF. Similar to the *DoubleOval_35kph*, the model-based approaches are more accurate, especially for the Solo MEKF and IKF, in which the biases are estimated. Unlike the *DoubleOval_35kph*, the fast cornering dynamic of the vehicle in the *LaneChangeISO* manoeuvres does not generate a large sideslip angle. Hence, the differences between the sideslip estimations in the Solo MEKF and the IKF are small, see Figure 6a.

Examining the heading estimations of the four estimation approaches, Figure 6b presents similar findings to those in the *DoubleOval_35kph*. While the 2DoF vehicle model fails to track the heading of the vehicle, the Solo MEKF corrects slowly. Moreover, the results show that approaches utilising the Triple KF, i.e. the Triple KF itself and the IKF, give better heading estimations. This is because of the corrected yaw rate from the *yawKKF* and the more accurate longitudinal velocity determination from *wssEKF*.

6. Conclusion

In this paper, an IKF is proposed to estimate the vehicle dynamics using low-cost GPS and INS. The IKF is composed of 4 KFs: *yawKKF*, *velKKF*, *wssEKF*, and MEKF. The *yawKKF* estimates the heading angle and yaw rate gyroscopic bias with the aid of GPS. These are then fed into the *wssEKF* with GPS velocities to estimate the tyre radius

bias and longitudinal velocity. With the corrected yaw rate measurement and a continuous source of longitudinal velocity, the *velKKF* improves the longitudinal velocity, and estimates the lateral velocity and accelerometer biases. These are then utilised in the MEKF (based on a 2DoF linear bicycle model) to estimate the steer bias as well as the sideslip and heading angle.

The performance of the IKF design is compared with the linear 2DoF bicycle model, the Triple KF and the Solo MEKF under 10 different simulated manoeuvres. From the results, it is found that, in general, MEKF is better for sideslip estimations and KKF is better for heading estimations. For fast dynamics, however, KKF suffers from continuous update and correction. Unless the update rate of reference sensors are increased, KKF is not superior to the MEKF in state estimations. By combining the MEKF and KKF (i.e IKF), the benefits of the two approaches are utilised. Results show that as long as the linear cornering coefficients are applicable to the vehicle model, the IKF is good at both sideslip and heading estimations.

Although the IKF is able to estimate the dynamic states of the vehicle for both types of manoeuvres, it is restricted to manoeuvres below 55kph. This speed limitation is because of the parameters in the MKF of the IKF design (particularly the cornering stiffnesses, $C_{y[ij]}$) are determined a priori using the linear tyre slip-force ratio. At a higher speed, the tyre forces do not vary linearly with slip, hence the vehicle dynamic estimations become inaccurate. For work in the future, it is recommended to combine the MEKF design of Wenzel (2005) with the proposed Triple KF, so the tyre force-slip ratio can be monitored continuously in real time. New or existing techniques for cornering stiffness estimation should also be investigated to enhance new designs of the IKF.

Nomenclature

$\circledast_b$	variable in the b-frame (vehicle body frame)
$\circledast_e$	variable in the e-frame (ENU frame)
$\hat{\circledast}$, $\circledast^{est}$	estimated variable
$\circledast^{gps}$, $\circledast_{gps}$	GPS measurements
$\circledast_{[ij]}$	variable at Front Right (FR), Front Left (FL), Rear Right (RR), Rear Left (RL) or variable at Front axle (F), Rear axle (R)
$\circledast_k$, $\circledast^k$	variable at time k
$\circledast_{k+1}$, $\circledast^{k+1}$	variable at time $k+1$
$\circledast_{k+1\|k}$	variable at time $k+1$, given information at time k
$\circledast_{max}$	maximum value in data set
$\circledast_{min}$	minimum value in data set
$\circledast^{ref}$	reference measurement
$\circledast^t$	true value
$\circledast_v$, $\circledast^v$	variable in the v-frame (vehicle dynamics frame)
$\circledast_{vel}$, $\circledast_{velKKF}$	variable of *velKKF*
$\circledast_{wss}$, $\circledast^{wssEKF}$	variable of *wssEKF*
$\circledast_{yaw}$, $\circledast_{yawKKF}$	variable of *yawKKF*
a	distance from centre of gravity to front axle
b	distance from centre of gravity to rear axle
b_d	bias due to the pitching motion
b_r	bias in the yaw rate gyroscope
b_w	bias of the tyre radius
$b_{w\|gps}$	estimated bias of the tyre radius given GPS measurements
b_x	bias in the longitudinal accelerometer
b_y	bias in the lateral accelerometer
b_δ	bias in the steer wheel angle
cg	centre of gravity
f	non-linear function for process matrix
g	non-linear function for measurement matrix
h	component of discrete measurement matrix, **H**
m	vehicle mass at centre of gravity
r_m	yaw rate gyro measurement
u	input vector
v	measurement noise vector
w	input disturbance vector
x	state vector
x	longitudinal displacement
$\dot{x}$	longitudinal velocity
$\ddot{x}$	longitudinal acceleration
y	lateral displacement
$\dot{y}$	lateral velocity
$\ddot{y}$	lateral acceleration
z	measurement vector
A	process matrix
A_x	longitudinal accelerometer measurement

A_y	lateral accelerometer measurement
$\mathbf{B}$	input matrix
$\mathbf{C}$	measurement matrix
$C_{y,[ij]}$	lateral tyre cornering stiffness
$F_{x,[ij]}$	Longitudinal force on tyre
$F_{y,[ij]}$	Lateral force on tyre
$\mathbf{F}$	Jacobian matrix for $\mathbf{f}$
$\mathbf{G}$	Jacobian matrix for $\mathbf{g}$
$\mathbf{H}$	discrete form of measurement matrix, $\mathbf{C}$
$\mathbf{I}$	identity matrix
$\mathbf{K}$	kalman filter gain matrix
$J_{[ij]}$	Second order moment of inertia about lateral axis of wheel
J_{zz}	Second order moment of inertia about vertical axis, Z_b
N	number of data points in set, X
$\mathbf{P}$	error covariance matrix
$\mathbf{Q}$	process covariance matrix
$R_{[ij]}$	wheel radius
$\mathbf{R}$	measurement covariance matrix
T_F	half of front track of vehicle
T_R	half of rear track of vehicle
T_s	sampling time
V	speed of vehicle at centre of gravity
$V_{[ij]}$	speed at the tyre
X	longitudinal axis
X	Data set
Y	lateral axis
$\alpha_{[ij]}$	slip angle at tyre
β	sideslip angle at the centre of gravity
$\beta_{[ij]}$	sideslip angle at the tyre
$\delta_{[ij]}$	steer angle on the tyres
ν	course angle about centre of gravity
$\omega_{[ij]}$	wheel rotational velocity at each wheel
ψ	Euler yaw angle
$\mathbf{\Gamma}_k$	discrete form of disturbance matrix
$\mathbf{\Delta}_k$	discrete form of input matrix, $\mathbf{B}$
$\mathbf{\Phi}_k$	discrete form of process matrix, $\mathbf{A}$

Acknowledgement

The authors would like to express their gratitude to Jaguar Land Rover and EPSRC for their support on this project.

Appendix A. Sensor parameters

Appendix A.1. Inertial Navigation System

Table A.3: Simulated INS errors

Sensor ($100Hz$)		**Standard deviation,** σ		**Bias**	
		Value	Unit	Value	Unit
Yaw rate gyroscope	r_m	1.0×10^{-1}	$deg/s.$	1.0	deg/s
Longitudinal accelerometer	$\ddot{x}_b$	5.0×10^{-1}	m/s^2	1.0	m/s^2
Lateral accelerometer	$\ddot{y}_b$	5.0×10^{-1}	m/s^2	1.0	m/s^2
Steering wheel sensor	δ_w	1.0	deg	5.0	deg
Wheel speed sensot	ω	4.0×10^{-2}	m/s	—	—

Appendix A.2. Global Positioning System

Table A.4: GPS errors based on DG-100 without an antenna

GPS ($1Hz$)		**Standard deviation,** σ
		Value
Eastings position	σ_{x_e}	3.0
Northings position	σ_{y_e}	3.0
Longitudinal velocity	$\sigma_{\dot{x}_e}$	2.5×10^{-2}
Lateral velocity	$\sigma_{\dot{y}_e}$	2.5×10^{-2}
Resultant velocity	σ_V	$\sqrt{\left(\frac{\dot{x}_e}{V}\sigma_{\dot{x}_e}\right)^2 + \left(\frac{\dot{y}_e}{V}\sigma_{\dot{y}_e}\right)^2}$
Tracking angle[1]	σ_ν	$\sqrt{\left(\frac{\dot{y}_e}{\dot{x}_e^2}\sigma_{\dot{x}_e}\right)^2 + \left(\frac{1}{\dot{x}_e}\sigma_{\dot{y}_e}\right)^2}$
	$\sigma_{\cos\nu}$	$\sqrt{\left(\sin\left(\frac{\dot{y}_e}{\dot{x}_e}\right)\left(\frac{\dot{y}_e}{\dot{x}_e^2}\right)\sigma_{\dot{x}_e}\right)^2 + \left(\sin\left(\frac{\dot{y}_e}{\dot{x}_e}\right)\left(\frac{1}{\dot{x}_e}\right)\sigma_{\dot{y}_e}\right)^2}$
	$\sigma_{\sin\nu}$	$\sqrt{\left(\cos\left(\frac{\dot{y}_e}{\dot{x}_e}\right)\left(\frac{\dot{y}_e}{\dot{x}_e^2}\right)\sigma_{\dot{x}_e}\right)^2 + \left(\cos\left(\frac{\dot{y}_e}{\dot{x}_e}\right)\left(\frac{1}{\dot{x}_e}\right)\sigma_{\dot{y}_e}\right)^2}$

[1] $\nu = \tan^{-1}\left(\frac{\dot{y}_e}{\dot{x}_e}\right) \approx \frac{\dot{y}_e}{\dot{x}_e}$

Appendix B. Vehicle Parameters

Table B.5: Vehicle parameters used for this project

	Value	Unit
Dimension		
distance from front axle to cg (a)	1.360	m
distance from rear axle to cg (b)	1.546	m
cg height	0.554	m
front track (T_F)	0.768	m
rear track (T_R)	0.768	m
Masses and inertia		
sprung mass (m_s)	1665.900	kg
unsprung mass per wheel (m_u)	48.080	kg
total mass of vehicle (m)	1858.000	kg
roll inertia about cg (J_{xx})	655.200	kgm^2
pitch inertia about cg (J_{yy})	3319.000	kgm^2
yaw inertia about cg (J_{zz})	3515.000	kgm^2
wheel inertia (J_w)	1.000	kgm^2
Steering		
On centre rack ratio	17.58	
Tyre		
wheel radius	0.329	m
Aerodynamics		
aerodynamic coefficient (C_{dx})	0.305	
frontal cross-sectional area (A_x)	2.200	m^2
air density (ρ)	1.205	kgm^{-3}

References

Anderson, R., Bevly, D., 2005. Estimation of tire cornering stiffness using GPS to improve model based estimation of vehicle states. In: Proceedings of IEEE Intelligent Vehicles Symposium. pp. 801–806.

Bakker, E., Pacejka, H., Lidner, L., 1989. A new tyre model with application in vehicle dynamics studies. In: Proceedings of the 4th Auto Technologies Conference. Monte Carlo, SAE paper 890087.

Bayliss, M., Leung, K.-T., Whidborne, J., Purdy, D., Williams, R., 2006. Four wheel steer controller development utilising a GPS (global positioning satellite) system compensated inertial sensor suite. In: Proceedings of FISITA World Automotive Congress. Yokohama, Japan.

Best, M., Gordon, T., Dixon, P., 2000. An extended adaptive Kalman filter for real-time state estimation of vehicle handling dynamics. Vehicle System Dynamics 34, 57–75.

Best, M., Newton, A., Tuplin, S., 2007. The identifying extended Kalman filter: parametric system identification of a vehicle handling model. In: Proceedings of the Institution of Mechanical Engineers, Part K (Journal of Multi-Body Dynamics). Vol. 221. pp. 87–98.

Bevly, D., Gerdes, J., Wilson, C., 2002. The use of GPS based velocity measurements for measurement of sideslip and wheel slip. Vehicle System Dynamics 38 (2), 127–47.

Bevly, D., Gerdes, J., Wilson, C., Zhang, G., 2000. The use of GPS based velocity measurements for improved vehicle state estimation. In: Proceedings of American Control Conference. Vol. 4. Chicago, USA, pp. 2538–2542.

Bevly, D., Sheridan, R., Gerdes, J., 2001. Integrating INS sensors with GPS velocity measurements for continuous estimation of vehicle sideslip and tire cornering stiffness. Proceedings of the American Control Conference 1, 25–30.

Blundell, M., Harty, D., 2004. The Multibody Systems Approach to Vehicle Dynamics, 1st Edition. Butterworth-Heinemann.

Cherouat, H., Braci, M., Diop, S., 2005. Vehicle velocity, side slip angles and yaw rate estimation. IEEE International Symposium on Industrial Electronics 1, 349–354.

Farmer, C., 2001. New evidence concerning fatal crashes of passenger vehicles before and after adding antilock braking systems. Accident Analysis and Prevention 33, 361–369.

Farmer, C., Lund, A., Trempel, R., Braver, E., 1997. Fatal crashes of passenger vehicles before and after adding antilock braking. Accident Analysis and Prevention 29 (6), 745–757.

Grewal, M., Weill, L., Andrews, A., 2007. Global Positioning Systems, Inertial Navigation, and Integration. Wilney.

Lawrence, A., 1998. Modern inertia technology, navigation guidance and control. Springer-Verlag.

Leung, K., Whidborne, J., Purdy, D., Dunoyer, A., 2009a. A review of ground vehicle dynamic state estimations utilising GPS/INS. Vehicle System Dynamics.

Leung, K., Whidborne, J., Purdy, D., Dunoyer, A., Williams, R., 2008. A study on the effect of GPS accuracy on a GPS/INS Kalman filter. In: Proceedings of UKACC International Conference on Control. Manchester, UK.

Leung, K.-T., Whidborne, J., Purdy, D., Dunoyer, A., SAE paper 2009-01-1287 2009b. Ideal vehicle sideslip estimation using consumer grade GPS and ins. SAE International.

Manning, W., Crolla, D., 2007. A review of yaw rate and sideslip controllers for passenger vehicles. Transactions of the Institute of Measurement and Control 29 (2), 117–135.

OXTS, 2008. Oxford technical solution.
URL `http://www.oxts.co.uk/`

Pacejka, H., Bakker, E., 1993. The magic formula tyre model, tyre models for vehicle dynamic analysis. In: Proceedings of the 1st International Colloquium on Tyre Models for Vehicle Dynamic Analysis. pp. 1–18.

Pacejka, H., Besselink, I., 1997. Magic formula tyre model with transient properties. In: Proceedings of the Berlin Tyre Colloquium, Vehicle System Dynamics Suppliment. Vol. 27. pp. 145–155.

Rock, K., Beiker, S., Laws, S., Gerdes, J., 2005. Validating GPS based measurements for vehicle control. In: 2005 ASME International Mechanical Engineering Congress and Exposition, IMECE 2005, Nov 5-11 2005. Vol. 74 DSC. pp. 583–592.

Ryu, J., Rossetter, J., Gerdes, J., 2002. Vehicle sideslip and roll parameter estimation using GPS. In: AVEC 2002 6th International Symposium on Advanced Vehicle Control. Hiroshima, Japan.

Van Zanten, A., 2002. Evolution of electronic control systems for improving the vehicle dynamic behaviour. In: Proceedings of International Symposium on Advanced Vehicle Control. Hiroshima, Japan.

Welch, G., Bishop, G., 2001. An introduction to the Kalman filter. Tech. rep., University of North Carolina at Chapel Hill.

Wenzel, T., 2005. State and parameter estimation for vehicle dynamic control. Ph.D. thesis, Coventry University.